Impact of deposition voltage on the physical properties of rare earth element doped strontium sulphide for optoelectronic application

S. O. Samuel[1, 3], C. K. Ojoba[2], E. P. Ogherohwo[3], I. L. Ikhioya[4, 5*]

[1]Department of Science Laboratory Technology, Delta State University, Abraka. Delta State
[2]Department of Physics, College of Education Warri, Delta State.
[3]Federal University of Petroleum Resources, Effurun, Delta State.
[4]Department of Physics and Astronomy, University of Nigeria, Nsukka, 410001, Enugu State, Nigeria
[5]National Centre for Physics, Quaid-i-Azam University Campus, Islamabad, 44000, Pakistan

ABSTRACT: In this study, electrochemical deposition was used to synthesize SrS-doped zirconium materials at a varying voltage of deposition. The XRD result shows that SrS/Zr has a prominent peak intensity corresponding to 2theta values of 26.45°, 33.86°, 38.01°, and 51.49°. The crystal lattice is shown by the prominent peak intensity with higher 2theta degree values; the appearance of an unindexed peak is caused by the substrate utilized for the deposition. SrS surface morphology reveals a Clove-like surface with precipitate visible in the SrS micrograph; the large grain size on the surface of the substrate exhibits photon absorption but lacks any signs of pinholes. At the introduction of zirconium as a dopant to the SrS precursor, there was a drastic change in the precursor which is also noticed on the surface micrograph of the analyzed films. The films show a decrease in thickness from 129.14 to 120.09 nm and an increase in film resistivity from 1.24 x 10^9 to 1.29 x 10^9 ohm.m, which further led to a decrease in conductivity from 8.06 x 10^8 to 7.75 x 10^8 S/m. The impact of the deposition voltage on the reflectance reveals that lower voltage will stabilize the reflectance of SrS/Zr which will be useful for photovoltaic applications. SrS has an energy bandgap of 1.50 eV while SrS/Zr with bandgap energy of 2.00 – 2.50 eV.

KEYWORDS: SrS, dopant, rare earth element, structural, bandgap energy

[Received Mar. 30, 2023; Revised Nov. 20, 2023; Accepted Nov. 21, 2023] Print ISSN: 0189-9546 | Online ISSN: 2437-2110

I. INTRODUCTION

One of the most well-known and significant substances is strontium sulphide, which belongs to the family of alkaline-earth sulphide. The volume dependence of the energy gap, the phonon spectrum, the optical characteristics, the structural phase stability, the elastic properties, and the metallization process have all been investigated by numerous groups (citations). They discovered that the material's most stable state at ambient temperature is the rock-salt phase of strontium sulphide (citation). Alkaline-earth sulphide is used as the host material in devices including magneto-optical systems and multicolor thin-film electroluminescent (Vijay, *et al.*, 2005). These devices consist of a thin film insulator and a suitable phosphor layer, and they operate between 50 V and 300 V (Yu, *et al.*, 2022, Ankush, *et al.* 2009, and Yiming, *et al.*, 2014). Some labs are producing rare earth-doped alkaline earth sulphide hosts for a full-color display. Interest in alternative and renewable energy has surged due to the growing energy crisis. The creation of high-performance thermoelectric materials is urgently required since electricity is usually regarded as a greener energy source and because thermoelectric materials have the potential to transform waste heat into power, lowering carbon dioxide and greenhouse gas emissions. Alternative energy sources include geothermal energy, hydropower, wind, biomass, sun, and hydroelectric (Kanoğlu, *et al*., 2020). The world is running out of usable energy from fossil fuels (oil, gas, coal, natural gas, and nuclear power) at the start of the twenty-first century, and renewable energies (wind and solar) are yet not well developed to provide a complete and flexible alternative. Due to the scarcity of fossil fuels and the majority of projections indicating that proven oil reserves won't be sufficient to supply global demand until at least the middle of the twenty-first century (Lisin, *et al*., 2018, Tishkov, *et al.*, 2020, Andryeyeya, *et al.*, 2021 and Ucal & Xydis 2020), humanity is currently moving toward dependence on renewable energy sources.

The operating wavelength of an optoelectronic device is influenced by the energy band gap of a semiconductor material. For applications like detectors, LEDs, solar cells, and

*Corresponding author: imosobomeh.ikhioya@unn.edu.ng
doi: http://dx.doi.org/10.4314/njtd.v18i4.1709

lasers, it is crucial to realize any desired band gap, or even spatially graded band gaps. Since III-V semiconductor materials and their alloys have a direct-band gap, they are frequently used to build optoelectronic devices, in contrast to the great majority of electrical devices, which are based on silicon (Nasr, *et al*., 2020, Aghahosseini & Breyer, 2018, Shao, *et al.*, 2017, Heine, 2015, and Samuel, *et al*., 2023). Our knowledge of the properties of these materials has tremendously facilitated the development of optoelectronic devices. Optoelectronic devices are widely employed in the fields of computer science, entertainment, lighting, and medicine. The biggest benefit to humanity may have come from the introduction of optical fiber communications, which allowed for the low-cost, high-quality transmission of voice and data around the globe (Ikhioya, *et al.*, 2023, Ikhioya, *et al.*, 2023, and Hao, *et al.*, 2004).

An extremely significant technology is the electrochemical deposition method combining layers of readily available, low-cost base materials with special metals that have similar properties. Their use is expanded to include jobs that would not have been feasible in previous circumstances (Aghahosseini & Breyer; 2018, Heine, 2015;, Carlie, *et al.*, 2010,; Akpu, *et al*., 2021;, Ikhioya, *et al*., 2020, Ikhioya, *et al.*, 2019;, Ikhioya, *et al*., 2020;, Ikhioya, *et al*., 2023,; Udofia, *et al*., 2022).

In this work, SrS-doped zirconium materials were produced electrochemically at varied deposition voltages. The materials' morphology, structural analysis, elemental content, and electrical characteristics were subsequently examined utilizing trusted characterization techniques.

II. EXPERIMENTAL DETAIL

Chemicals that have been evaluated analytically are purchased and used without further purification. Fluorine-doped Tin Oxide (FTO) conductive glass served as the substrate. The substrates underwent acetone and methanol immersion, distilled water washing, and a 30-minute treatment with an ultrasonic bath in acetone. After being cleansed in distilled water, they were baked to dry. Thioacetamide (C_2H_5NS), 0.1 mol of strontium chloride hexahydrate ($SrCl_2.6H_2O$), and 0.01 mol of Zirconium (IV) oxychloride octahydrate ($ZrOCl_2.8H_2O$) were utilized as the cationic, anionic, and dopant concentrations. The films were deposited using the electrochemical deposition process. The electrochemical apparatus had a bath that included distilled water, 20 ml of each cationic and anionic precursor, and a 100 ml beaker. The cathode and anode materials were fluorine-doped tin oxide and carbon, and direct current voltage was generated by the power supply. The chamber has three electrode configurations: a working electrode, an electrode made of silver-silver chloride (Ag/AgCl), which serves as the reference electrode, and platinum mesh as the positive electrode. For all depositions, the fluorine-doped tin oxide substrate was positioned perpendicular to the chamber, including the counter and reference electrodes. For 10 seconds, the synthesis was conducted at a potentiostat setting of 200 mV against SCE. As a result, the synthesized films were cleaned and dried. The target materials, which consist of equal amounts (20 ml) of strontium chloride, thioacetamide, and 10 ml of silver nitrate solutions, were metered into the beakers during the deposition process. After the syntheses, the films were heated and annealed for 30 minutes to remove concentrated tensions under a variable voltage supply of 10V to 14V. By adding 10 ml of 0.01 mol of silver nitrate to the electrochemical bath, the silver nitrate dopant was introduced. The samples were collected at pH levels of 7.0 and room temperature. Scanning electron microscopy, DW-XRD 2700A X-ray diffractometer with Cu-Kα line (λ = 1.54184 Å) in 2θ range from 10° - 80°, a four-point probe (Model T345), and a UV-1800 visible spectrophotometer were used to characterize the prepared SrS and SrS/Ag films for their surface morphological, structural, elemental, electrical, and optical properties.

III. RESULT AND DISCUSSIONS

A. Structural analysis of SrS and SrS doped zirconium

The crystalline structure of SrS and SrS doped zirconium in Figure 1 was determined using XRD. The spectrum is polycrystalline with a cubic structure and a prominent peak at (111) orientation for the films. Strontium sulphide doped zirconium synthesized at various voltages has a prominent peak intensity corresponding to 2theta values of 26.45^o, 33.86^o, 38.01^o, and 51.49^o. The crystal lattice is shown by the prominent peak intensity with higher 2theta degree values; the appearance of an unindexed peak is caused by the substrate utilized for the deposition. Because of their nature, polycrystalline materials are continuously better for making optoelectronic devices (citation). The spectrum suggests that the higher deposition voltage reduces peak intensities of the synthesized material may result from the film's decreased thickness, which increases the available surface area for photovoltaic and solar cell activities. Table 1 includes additional structural value and the average crystallite size of the films in addition to the computed crystallite or grain sizes, dislocation density, and deposition voltage for the films deposited (Samuel, *et al.*, 2023). Using XRD data, Figure 1b shows (β cos θ) as a function (Sin θ). The Williamson-Hall plot's slope rises as deposition voltage increases. As a result of strain hardening, the dislocation density increases, the crystallite size varies, and the obvious peak of the diffraction angle expands. Figure 1c displays a plot of the crystallite size of the deposited material as a function of the 2-theta. The plot showed that the material fluctuated as the 2theta increased, in contrast to the voltage of deposition-dependent variation of the material. The diffraction angle rises as the crystallite size increases.

B. Surface morphology of SrS and SrS doped zirconium

The micrograph of SrS and SrS/Zr in Figure 2 shows agglomeration on the films without pinholes and large grain size or nanoparticles. SrS surface morphology reveals a Clove-like surface with precipitate visible in the SrS micrograph; the large grain size on the surface of the substrate exhibits photon absorption but lacks any signs of pinholes. At the introduction of zirconium as a dopant to the SrS precursor, there was a drastic change in the precursor which is also noticed on the surface micrograph of the analyzed films. Cloudlike precipitate

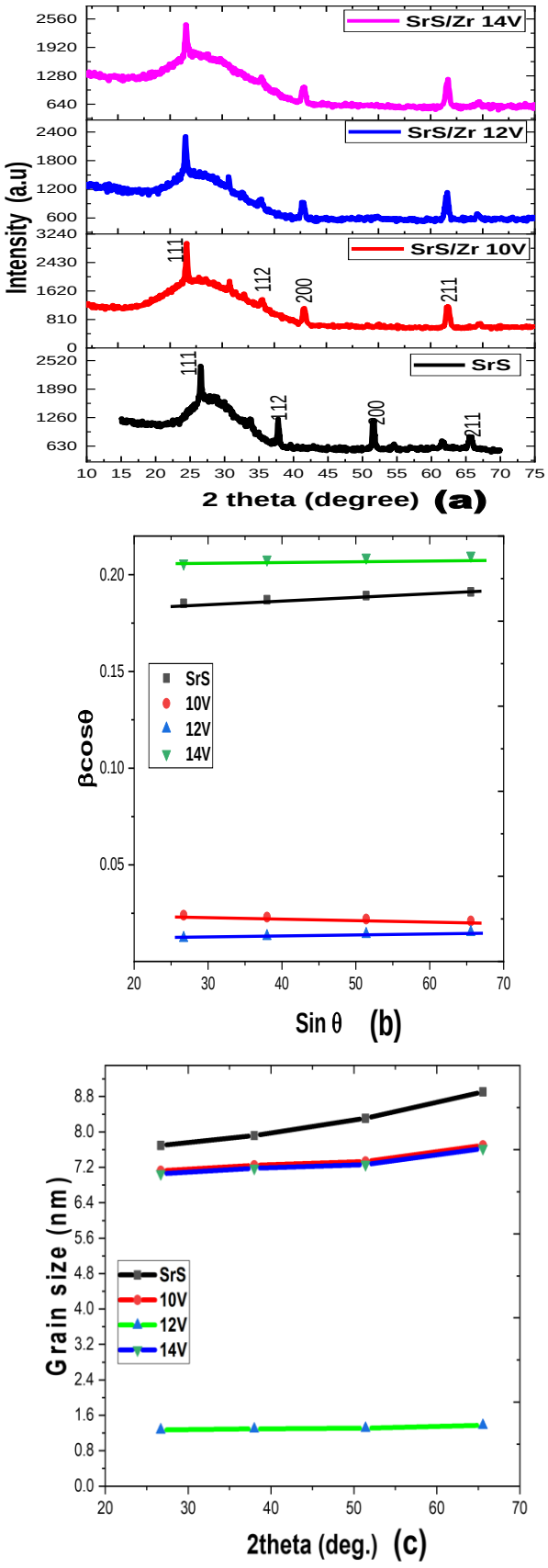

Figure 1: XRD spectrum [a], Williamson-Hall plot [b], Grain size against 2-theta [c]

was observed and it has shown on the surface morphology of the films. As the deposition voltage increase the cloudlike precipitate recircled and formed a thick cloud on the surface of the films (Samuel *et al.*, 2023). The doped SrS material displayed homogeneous deposition with nanoparticles that covered the whole substrate for photovoltaic application. The surface micrograph of the zirconium doped films is well structured on the surface of the FTO substrate used for the synthesis without any crack or lattice strain and they will make a good candidate for photovoltaic and other applications in the electronic industries. Figure 3 depicts the elemental spectrum of SrS and SrS doped zirconium films. From the spectrum, itis evident that strontium, sulphide, and the dopant zirconium are shown with prominent peaks. The others element seen on the spectrum is the elemental made up of the FTO substrate used for the synthesis. Table 2.

C. The resistivity and conductivity analysis of SrS and SrS/Zr

The resistivity and conductivity of SrS and SrS/Zr are shown in Table 3. The films show a decrease in thickness (t) from 129.14 to 120.09 nm and an increase in film resistivity from 1.24 x 10^9 to 1.29 x 10^9 ohm.m, which further led to a decrease in conductivity from 8.06 x 10^8 to 7.75 x 10^8 S/m (Samuel, *et al.*, 2023). The low resistivity and high conductivity of the synthesized films made them suitable for photovoltaic and solar cell applications (citations). Any reason for the increase at SrS/Zr14V. Figure 4 (a) demonstrates low resistivity and high conductivity as film thickness decreases. Resistivity and conductivity are plotted against deposition voltage in Figure 4 (b), which provides a nonlinear graph and demonstrates how resistivity and conductivity increase and decrease as the deposition voltage increases.

D. Optical study of SrS and SrS/Zr

Figure 5 illustrates the absorbance, transmittance, reflectance, and energy bandgap of SrS and SrS/Zr.The absorbance in Figure 5 (a) depicts a decrease in the absorbance and an increase in the light radiation (wavelength) that passes through the film during scanning. The film without zirconium reveals the highest absorbance in the spectra which is useful for emitting systems in the electronic industries and while the zirconium dopant was introduced the absorbance of the films decreased and stabilizes in both regions of electromagnetic radiation. The ultraviolet region records an increase in the absorbance and decreases down the infrared region of the spectra. The deposition voltage also has an impact on the film, an increase in the voltage lead to a decrease in the absorbance of the films and a higher deposition voltage will further depreciate the absorbance of SrS/Zr. The absorbance of SrS/Zr will be useful for optoelectronic applications. The transmittance in Figure 5 (b) shows that an increase in the light radiation (wavelength) leads to an increase in the transmittance of the films (Samuel *et al.*, 2023). The impact of the deposition voltage on the transmittance reveals that lower voltage will stabilize the transmittance of SrS/Zr which will be useful for photovoltaic applications. The reflectance in Figure 5 (c) shows an increase in the reflectance of the SrS without zirconium and a decrease in the reflectance of SrS doped zirconium. The impact of the deposition voltage on the

Table 1: Structural values of SrS and SrS/Zr

films	2θ (deg.)	d (spacing) Å	(Å)	(β)	(hkl)	(D) nm	σ lines/m^2
SrS	26.6971	3.3360	5.7781	0.1852	111	7.6958	5.1445
	37.9741	2.3672	4.7345	0.1871	112	7.9188	4.9700
	51.3944	1.7762	3.5524	0.1892	200	8.3100	4.8648
	65.5611	1.4225	3.1809	0.1911	211	8.9066	4.3940
SrS/Zr 10V	26.4569	3.3657	5.8296	0.0240	111	7.1217	6.0060
	33.8661	2.6444	5.2888	0.0230	112	7.2469	5.8003
	38.0166	2.3647	4.7294	0.0220	200	7.3326	5.6656
	51.4973	1.7729	3.9644	0.0210	211	7.6971	5.1418
SrS/Zr 12V	26.4569	3.3657	5.8296	0.0122	111	1.2717	1.8835
	33.8661	2.6444	5.2888	0.0132	112	1.2941	1.8189
	38.0166	2.3647	4.7294	0.0142	200	1.3094	1.7767
	51.4973	1.7729	3.9644	0.0152	211	1.3744	1.6124
SrS/Zr 14V	26.4569	3.3657	5.8296	0.2059	111	7.0547	6.1207
	33.8661	2.6444	5.2888	0.2079	112	7.1787	5.9110
	38.0166	2.3647	4.7294	0.2089	200	7.2636	5.7737
	51.4973	1.7729	3.9644	0.2099	211	7.6247	5.2412

Note: d lattice spacing;

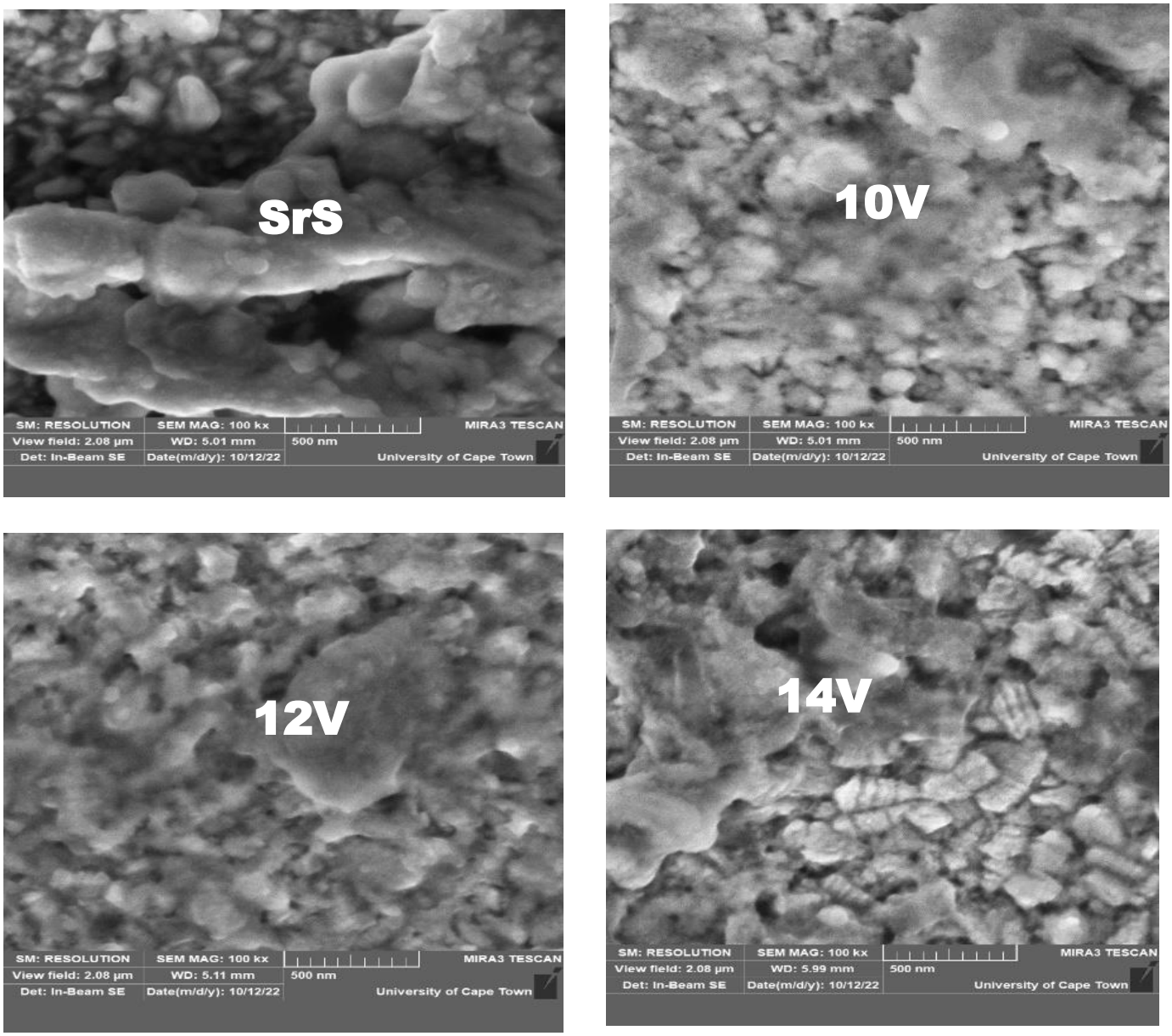

Figure 2: The surface image of (a) SrS and SrS/Zr at (b) 10V, (c) 12V and (d) 14V.

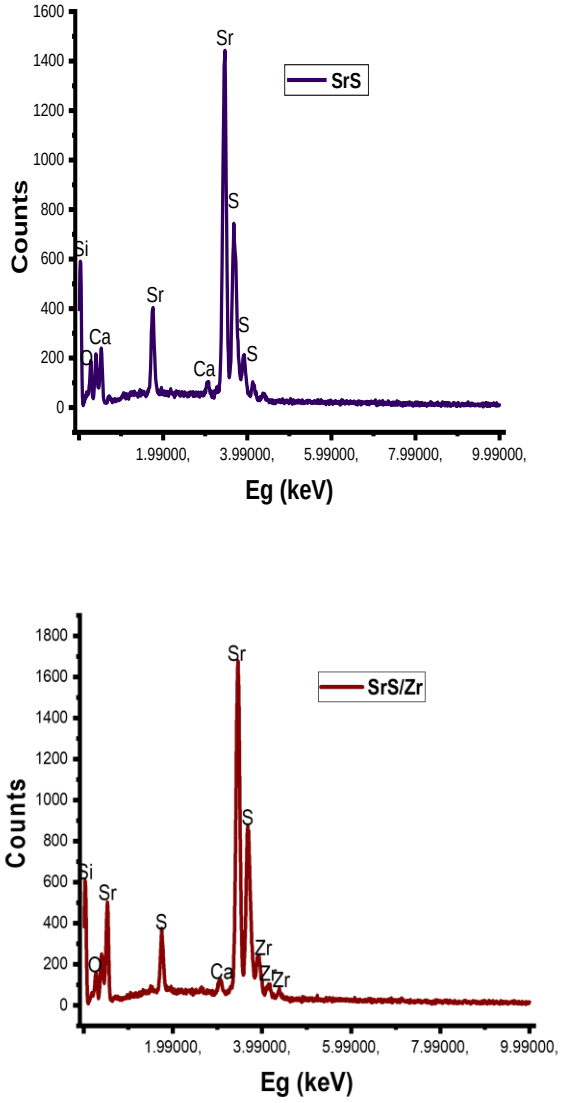

Figure 3: EDX spectrum of SrS and SrS/Zr

Table 2: EDX spectra atomic weight percentages of the constituent elements.

Strontium Sulphide		Strontium Sulphide doped Silver	
Elements	Atomic Weight (%)	Elements	Atomic Weight (%)
Sr	60.06	Sr	60.37
S	20.02	S	17.00
Si	9.92	Zr	08.01
Ca	5.99	O	03.00
O	4.01	Ca	02.60
-	-	Si	09.01

reflectance reveals that lower voltage will stabilize the reflectance of SrS/Zr, which will be useful for photovoltaic applications. Figure 5 (d) is the energy bandgap, which shows that SrS has an energy bandgap of 1.50 eV while SrS/Zr has a bandgap energy of 2.00 – 2.50 eV.

Table 3: Electrical parameters of SrS and SrS doped zirconium

Films	t (nm)	ρ (Ω.m) × 10^9	σ (S/m)$^{-1}$ ×10^8
SrS	125.02	1.32	7.57
SrS/Zr 10V	129.14	1.24	8.06
SrS/Zr 12V	120.20	1.27	7.87
SrS/Zr 14V	121.09	1.29	7.75

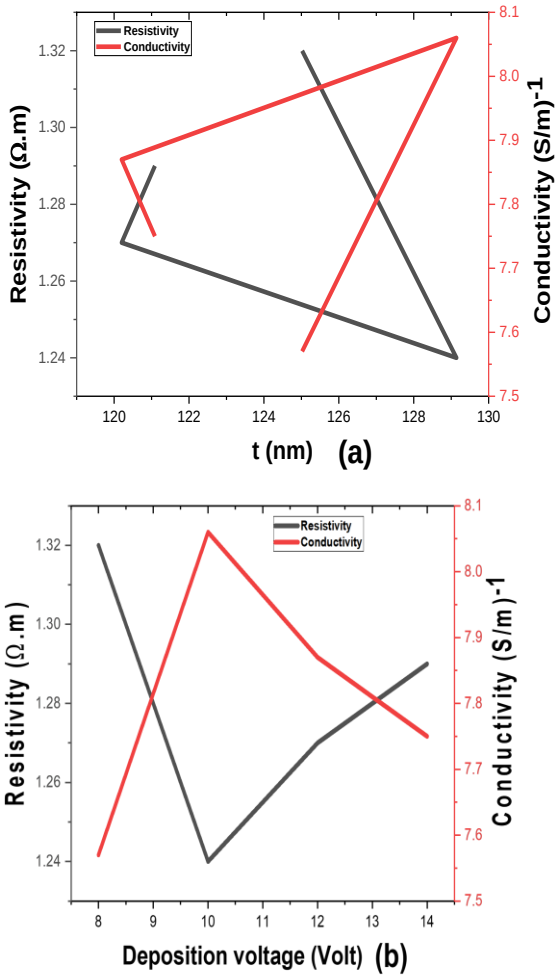

Figure 4: resistivity, conductivity vs thickness (a), and deposition voltage (b)

The refractive index, extinction coefficient, and optical conductivity of SrS and SrS/Zr are shown in Figure 6. Figure 6 (a) is the refractive index synthesized at various deposition voltages. An increase in the reflective index led to an increase in the photon energy of the films. The zirconium dopant and the deposition voltage showed a great impact on the film synthesis. It was observed that lower voltage will improve the refractive index of the films (Samuel *et al.*, 2023). Figure 6 (b) is the extinction coefficient synthesized at various deposition voltages, an increase in the extinction coefficient led to an increase in the photon energy of the films. The zirconium dopant and the deposition voltage showed a great impact on the film synthesis. It was noticed that lower voltage will improve the extinction coefficient of the films.

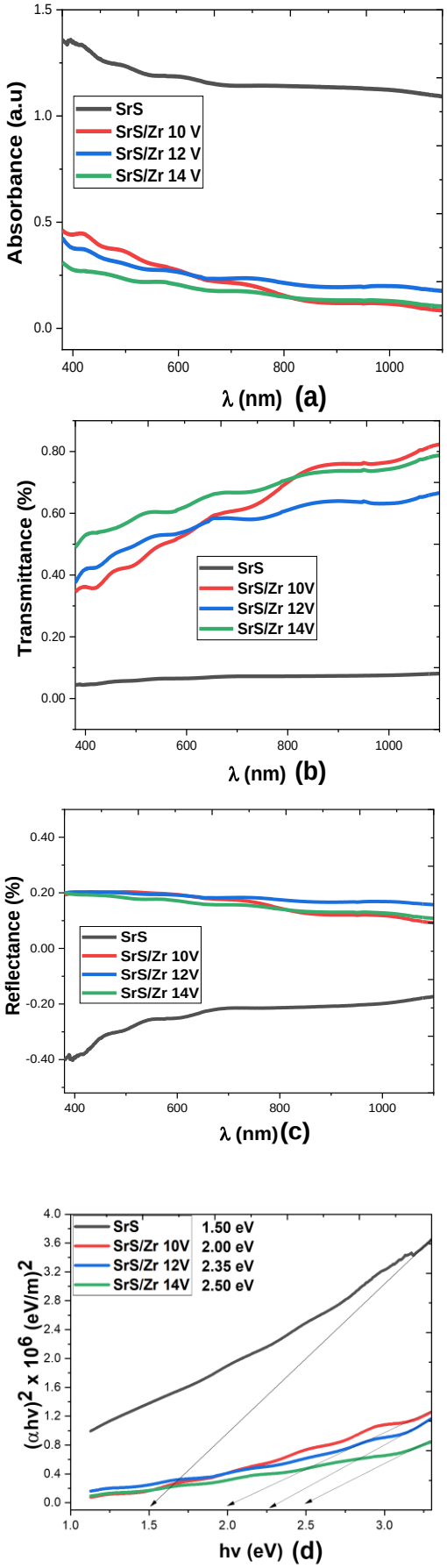

Figure 5: Absorbance (a), transmittance (b), reflectance (c), and energy bandgap (d) of SrS and SrS/Zr

Figure 6 (c) is the optical conductivity synthesized at various deposition voltages, an increase in the optical conductivity led to an increase in the photon energy of the films. The zirconium dopant and the deposition voltage showed a great impact on the film synthesis. It can be observed that lower voltage will improve the optical conductivity of the films.

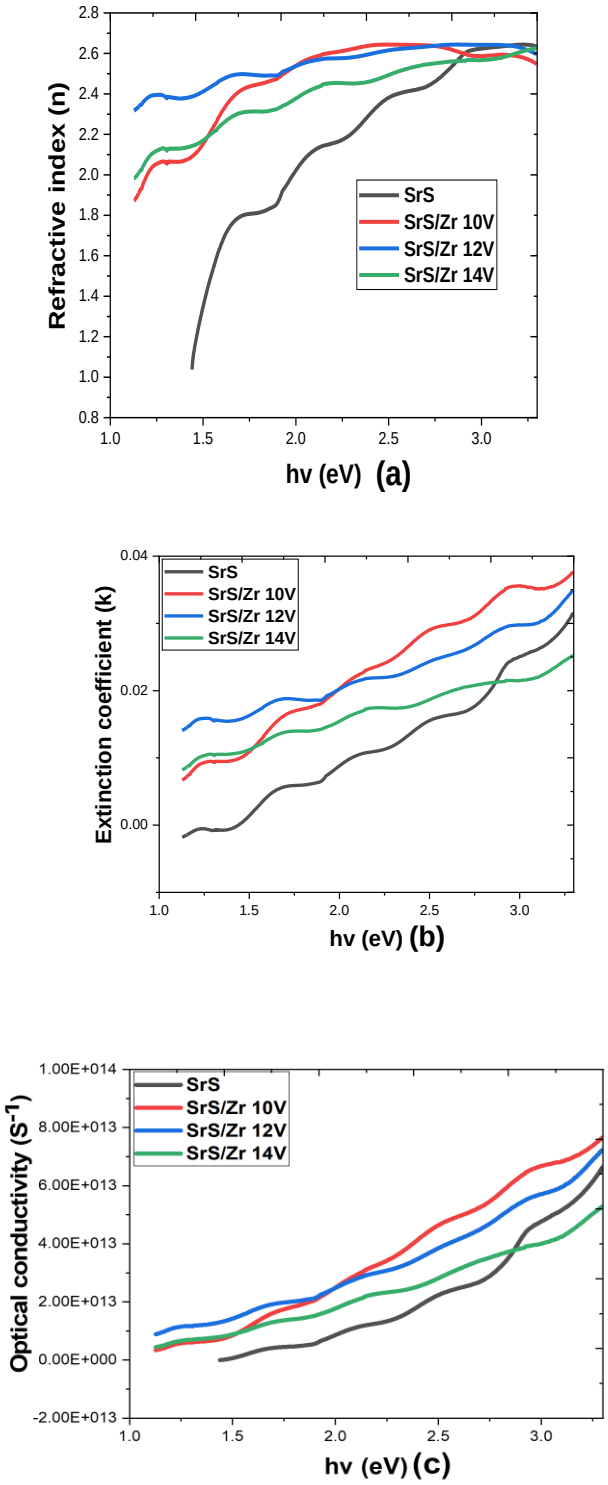

Figure 6: Refractive index (a), extinction coefficient (b), and optical conductivity (c).

Figure 7 depicts the real and imaginary dielectric constant of SrS and SrS/Zr films synthesized at different deposition voltages. Figure 7 (a) is the real part of SrS/Zr, which shows that as the photon energy rises, the real part of the dielectric material increases. The impact of the zirconium and deposition voltage was detected on the spectra. It was observed that lower voltage will enhance the real part of the dielectric material (Samuel *et al.*, 2023). On the other hand, Figure 7 (b) is the imaginary part of SrS/Zr, which shows that as the photon energy rises the imaginary part of the dielectric material increases. The impact of the zirconium and deposition voltage was detected on the spectra, and it was observed that a lower voltage will improve the imaginary part of the dielectric material.

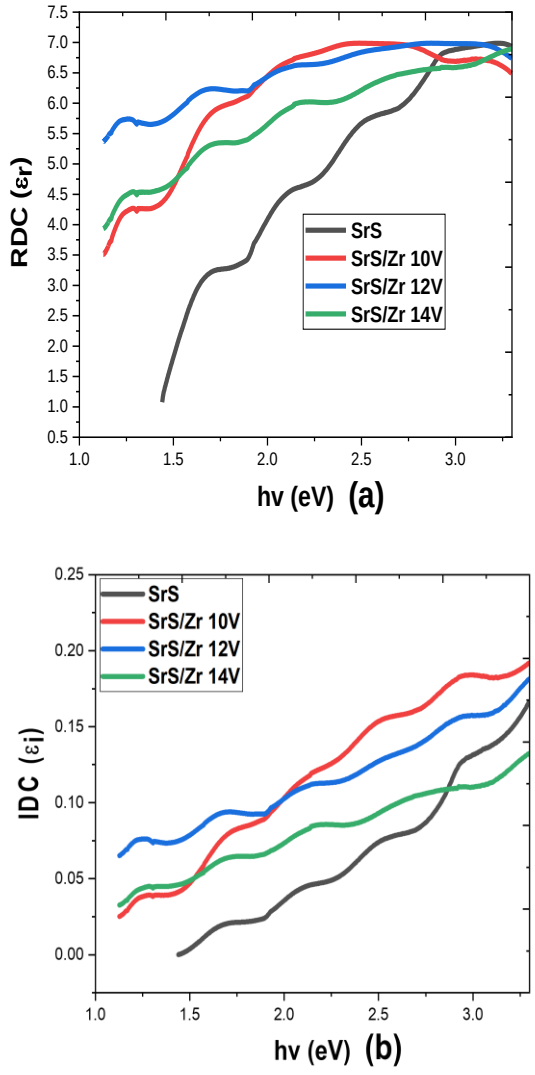

Figure 7: Real (a), and imaginary (b)

IV. CONCLUSION

We have successfully synthesized strontium sulphide-doped zirconium via an electrochemical deposition process at varied deposition voltages. The XRD result shows that SrS/Zr has a prominent peak intensity corresponding to 2theta values of 26.45º, 33.86º, 38.01º, and 51.49º. The crystal lattice is shown by the prominent peak intensity with higher 2theta degree values. The appearance of an unindexed peak is caused by the substrate utilized for the deposition. SrS surface morphology reveals a clove-like surface with precipitate visible in the SrS micrograph; the large grain size on the surface of the substrate exhibits photon absorption but lacks any signs of pinholes. At the introduction of zirconium, as a dopant to the SrS precursor, there was a drastic change in the precursor which is also observed on the surface micrograph of the analyzed films. The films show a decrease in thickness from 129.14 to 120.09 nm and an increase in film resistivity from 1.24 x 10^9 to 1.29 x 10^9 ohm.m, which further led to a decrease in conductivity from 8.06 x 10^8 to 7.75 x 10^8 S/m. The impact of the deposition voltage on the reflectance reveals that lower voltage will stabilize the reflectance of SrS/Zr, which will be useful for photovoltaic applications. SrS has an energy bandgap of 1.50 eV, while the SrS/Zr has with bandgap energy of 2.00 – 2.50 eV.

AUTHOR CONTRIBUTIONS

S. O Samual, C. K Ojoba, and E. P Ogherohwo: Conceptualization, Software, Validation, Writing – original draft. **I. L Ikhioya and E. P Ogherohwo:** Conceptualization, Methodology, Supervision. **S. O Samual and I. L. Ikhioya:** Writing – review & editing.

REFERENCES

Aghahosseini, A. and Breyer, C. (2018). Assessment of geological resource potential for compressed air energy storage in global electricity supply. *Energy Convers. Manag. 169*, 161–173.

Akpu, N. I.; A.D. Asiegbu; L. A. Nnanna; I. L. Ikhioya; T. L. Mgbeojedo. (2021). Investigation on the Influence of Varying Substrate Temperature on the Physical Features of Yttrium Doped Cadmium Selenide Thin Films Materials," SSRG International Journal of Applied Physics, vol. 8, no. 2, pp. 37-46,. https://doi.org/10.14445/23500301/IJAP-V8I2P106.

Andryeyeva, N.; O. Nikishyna; B. Burkynskyi; N. Khumarova; O. Laiko and H. Tiutiunnyk. (2021). Methodology of analysis of the influence of the economic policy of the state on the environment. Insights Reg. Dev., 3, 198–212.

Carlie, N. ; J. D. Musgraves; B. Zdyrko; I. Luzinov; J. Hu; V. Singh; A. Agarwal; Kimerling; A. Canciamilla; F. Morichetti and K. Richardson. (2010). Integrated chalcogenide waveguide resonators for mid-IR sensing: leveraging material properties to meet fabrication challenges. *Optics express*, *18*(25), 26728-26743.

Chen, Y.; S. W. Fan and G. Y. Gao. (2022). The SrS doped with Cl and K: a promising ambipolar semiconductor for transparent electronics application. *Journal of Physics D: Applied Physics*, *55*(45), 455108.

Hao, E.; S. Li; R. C. Bailey; S. Zou; G. C. Schatz and J. T. Hupp. (2004). Optical properties of metal nanoshells. *The Journal of Physical Chemistry B*, *108*(4), 1224-1229.

Heine, T. (2015). Transition metal chalcogenides: ultrathin inorganic materials with tunable electronic properties. *Accounts of chemical research*, *48*(1), 65-72.

Ikhioya, I. L.; F. U. Ochai-Ejeh and C. I. Uruwah. (2023). Impact of modulated temperature on photovoltaic properties of automated spray fabricated zirconium doped cobalt selenide films. *Materials Research Innovations*, 1-10.

Ikhioya, I. L.; E. U. Onoh; D. N. Okoli and A. J. Ekpunobi. (2023). Impact of bismuth as dopant on ZnSe material syntheses for photovoltaic application. *Materials Research Innovations*, 1-9.

Ikhioya, I.L.; G. M. Whyte and A. C. Nkele. (2023). Temperature-Modulated Nanostructures of Ytterbium-Doped Cobalt Selenide (Yb-CoSe) for Photovoltaic Applications," Journal of the Indian Chemical Society, vol. 100, no. 1, p. 100848, https://doi.org/10.1016/j.jics.2022.100848.

Ikhioya, I. L.; D. N. Okoli and A. J. Ekpunobi. (2020). (2020). Effect of Precursor pH on Cadmium Doped Manganese Sulphide (CdMnS) Thin Films for Photovoltaic Application," SSRG International Journal of Applied Physics, vol. 6, no. 2, pp. 1-8. https://doi.org/10.14445/23948884/IJMSE-V6I2P101.

Ikhioya, I. L.; D. N. Okoli and A. J. Ekpunobi. (2019). Effect of Temperature on SnZnSe Semiconductor Thin Films for Photovoltaic Application," SSRG International Journal of Applied Physics, vol. 6, no. 2, pp. 55-67,. https://doi.org/10.14445/23500301/IJAP-V6I2P109.

Ikhioya I. L.; M. C. Ezeorba; D. O. Okoroh; C. R. Anene and C. O. Obasi. (2020). The Influence of Precursor Temperature on the Properties of Erbium-Doped Zirconium Telluride Thin Film Material via Electrochemical Deposition," SSRG International Journal of Applied Physics, vol. 7, no. 1, pp. 102-109, http://dx.doi.org/10.14445/23500301/IJAP-V7I1P115.

Kanoğlu, M.; Y.A. Çengel and J.M. Cimbala. (2020). Fundamentals and Applications of Renewable Energy; McGraw-Hill Education: New York, NY, USA.

Lisin, E.; D. Shuvalova; I. Volkova; W. Strielkowski. (2018). Sustainable Development of regional power systems and the consumption of electric energy. *Sustainability*, *10*, 1111.

Nasr, A.K.; M.K. Kashan; A. Maleki; N. Jafari and H. Hashemi. (2020). Assessment of barriers to renewable energy development using stakeholders approach. *Entrep. Sustain. Issues , 7*, 2526–2541.

Samuel, S.O.; F. M. Lagbegha-ebi; E.P. Ogherohwo; A. Ekpekpo; J.T. Zhimwang and I.L. Ikhioya. (2023). Influence of deposition voltage on strontium sulphide doped silver for optoelectronic application,East Eur. J. Phys. 1, 189, https://doi.org/10.26565/2312-4334-2023-1-25.

Shao, Y.; X. Shi and H. Pan. (2017). Electronic, magnetic, and catalytic properties of thermodynamically stable two-dimensional transition-metal phosphides. *Chemistry of Materials*, *29* (20), 8892-8900.

Singh, V.; T. K. Gundu Rao; J. J. Miao and J. J. Zhu. (2005). Synthesis and characterization of Ce-doped SrS phosphors. *Radiation Effects & Defects in Solids*, *160*(7), 265-274.

Tishkov, S.; A. Shcherbak; V. Karginova-Gubinova; A. Volkov; A. Tleppayev and A. Pakhomova. (2020). Assessment the role of renewable energy in socio-economic development of rural and Arctic regions. *Entrep. Sustain. Issues, 7*, 3354–3368.

Ucal, M. and Xydis, G. (2020). Multidirectional relationship between energy resources, climate changes and sustainable development: Technoeconomic analysis. *Sustain. Cities Soc. , 60*, 102210.

Udofia K. I.; I. L Ikhioya; A. U. Agobi; D. N. Okoli and A. J. Ekpunobi. (2022). Effects of Zirconium on Electrochemically Synthesized Tin Selenide Materials on Fluorine Doped Tin Oxide Substrate for Photovoltaic Application," Journal of the Indian Chemical Society, vol. 99, no. 10, p. 10077, https://doi.org/10.1016/j.jics.2022.100737.

Vij, A.; S. Singh; R. Kumar; S. P. Lochab; V. V. S. Kumar and N. Singh. (2009). Synthesis and luminescence studies of Ce doped SrS nanostructures. *Journal of Physics D: Applied Physics*, *42*(10), 105103.

Zhao, Y.; F. T. Rabouw; T. V. Puffelen; C. A. V. Walree; D. R. Gamelin; C. de Mello Donegá and A. Meijerink. (2014). Lanthanide-doped CaS and SrS luminescent nanocrystals: a single-source precursor approach for doping. *Journal of the American Chemical Society*, *136*(47), 16533-16543.